HHS Public Access

Author manuscript

NMR Biomed. Author manuscript; available in PMC 2018 July 01.

Published in final edited form as:

NMR Biomed. 2017 July ; 30(7): . doi:10.1002/nbm.3721.

Detecting in vivo urokinase Plasminogen Activator activity with a catalyCEST MRI contrast agent

Sanhita Sinharay[1], **Christine M. Howison**[3], **Amanda F. Baker**[2], and **Mark D. Pagel**[1,2,3,*]

[1]Department of Chemistry and Biochemistry, University of Arizona, Tucson, AZ

[2]University of Arizona Cancer Center, University of Arizona, Tucson, AZ

[3]Department of Medical Imaging, University of Arizona, Tucson, AZ

Abstract

Urokinase plasmogen activator (uPA) promotes tumor invasion and metastasis. The monitoring of uPA activity using molecular imaging may have prognostic value and be predictive for response to anti-cancer therapies. However, the detection of *in vivo* enzyme activity with molecular imaging remains a challenge. To address this problem, we designed a nonmetallic contrast agent, GR-4Am-SA, that can be detected with Chemical Exchange Saturation Transfer Magnetic Resonance Imaging (CEST MRI). This agent has a peptide that is cleaved by uPA which causes a CEST signal at 5.0 ppm to decrease, and also has a salicylic acid moiety that can produce a CEST signal at 9.5 ppm which is largely unresponsive to enzyme activity. The two CEST signals were used to determine a reaction coordinate, representing the extent of enzyme-catalyzed cleavage of the GR-4Am-SA agent during an experimental study. Initial biochemical studies showed that GR-4Am-SA could detect uPA activity in reducing conditions. Subsequently, we used our catalyCEST MRI protocol with the agent to detect the uPA catalysis of GR-4Am-SA in a flank xenograft model of Capan-2 pancreatic cancer. The results showed an average reaction coordinate of 80% ± 8%, which was strongly dependent on the CEST signal at 5.0 ppm. The relative independence of the reaction coordinate on the CEST signal at 9.5 ppm showed that the detection of enzyme activity was largely independent of the concentration of GR-4Am-SA within the tumor tissue. These results demonstrated the advantages of a single CEST agent with biomarker-responsive and unresponsive signals for reliably assessing enzyme activity during *in vivo* cancer studies.

Corresponding Author: Mark D. Pagel, University of Arizona Cancer Center, 1515 N. Campbell Avenue, Tucson, AZ 85724-5024, Tel: (520)-404-7049, Fax: (520)-626-0395, mpagel@u.arizona.edu.

The current address for Dr. Sanhita Sinharay: National Institutes of Health, Bldg 10, IC 370, 10 Center Drive, Bethesda, MD 20815-9692

Co-Authors: Sanhita Sinharay, Chemistry and Biochemistry, University of Arizona, 1515 N. Campbell Avenue, Tucson, AZ 85724-5024, sinharay@email.arizona.edu

Christine M. Howison, University of Arizona Cancer Center, 1515 N. Campbell Avenue, Tucson, AZ 85724-5024, chowison@email.arizona.edu

Amanda F. Baker, University of Arizona Cancer Center, 1515 N. Campbell Avenue, Tucson, AZ 85724-5024, abaker@uacc.arizona.edu

Conflict of interest disclosure statement

The authors declare no conflicts of interest with regard to this research study.

SUPPORTING INFORMATION

Additional supporting information can be found in the online version of this article at the publisher's web site.

Keywords

CEST MRI; enzyme activity; urokinase Plasminogen Activator; pancreatic cancer

INTRODUCTION

Urokinase plasminogen activator (uPA) is a serine protease that contributes to cancer invasion and metastasis (1). For example, high levels of uPA can predict poor outcome for patients with breast cancer who are undergoing adjuvant treatment (2). Importantly, uPA is initially expressed, secreted, and bound to a uPA receptor as an inactive pro-uPA zymogen (Fig. 1) (3). The interaction of uPA with its receptor causes uPA to become active and subsequently catalyze the activation of other proteases. As an example, uPA catalyzes the conversion of plasminogen to plasmin, which rapidly degrades the extracellular matrix in the tumor microenvironment. In this context, the activation of uPA serves as an important control point to initiate a cascade of protease activities that promote tumor invasion and metastasis. Therefore, methods for interrogating uPA activity have strong potential to improve cancer diagnoses.

Historically, *ex vivo* diagnostic assays that measure uPA activity are infrequently used due to the challenges of collecting fresh tissue samples. Furthermore, uPA activity is unstable especially under oxidative conditions, which requires tissue samples to be analyzed soon after excision (4). uPA activity may be sensitive to environmental conditions, and tissue processing methods may compromise the extracellular tumor microenvironment (5). The collection and analysis problems of measuring uPA activity could potentially be overcome with noninvasive molecular imaging techniques that directly measure enzyme activity *in vivo* without disturbing the tumor microenvironment. Molecular imaging also has excellent potential to provide longitudinal assessments, which can have potentially profound impacts on monitoring the progression of suspicious lesion, monitoring the durability of anti-cancer treatments that target pathways upstream of uPA activation, and monitoring cancer patients who are in remission.

Chemical Exchange Saturation Transfer (CEST) MRI is a molecular imaging methodology that involves selective saturation of the MR signal of a proton on an agent, followed by chemical exchange of the agent's proton to a water molecule (Fig. 2) (6). This process results in a transfer of the saturation from the agent to water that can be detected using standard MRI acquisition methods. An enzyme-catalyzed change to the agent can change the chemical exchange rate of the proton transfer from the agent to water, which can alter the amplitude of the CEST signal (7). The agent can include another labile proton that can generate a CEST signal and is unresponsive to the enzyme catalysis, which can be used as a control signal to account for the concentration of the agent and other effects that influence CEST. The rapid MRI acquisition and comparison of these two CEST effects can be used to detect enzyme activity, which is known as catalyCEST MRI (8). In this study, we proposed to use catalyCEST MRI to detect uPA activity in a xenograft mouse model of Capan-2 pancreatic cancer.

We have previously reported a different CEST agent that was responsive to uPA enzyme activity (9). However, this agent only had an enzyme responsive CEST signal, requiring the co-injection of a second, enzyme-unresponsive CEST agent that was used as a control signal. The co-injection strategy halved the maximum dose of the enzyme-responsive CEST agent that could be administered. In our present study, we proposed to develop a single CEST agent with enzyme responsive and unresponsive signals that can detect uPA activity, which can allow for a higher maximum dose of agent relative to our previous study. Furthermore, our previous agent contained a paramagnetic metal ion, which limited the agent's concentration that could be administered to a mouse model. In our current study, we designed a diamagnetic agent that could be intravenously administered at a higher dose, which can potentially improve the sensitivity of detecting the agent during *in vivo* imaging studies.

METHODS AND MATERIALS

Chemical synthesis

The CEST agent, Gly-Arg-4-aminosalicylic acid (GR-4Am-SA)**,** was synthesized in five steps, and the intermediates and final product were characterized with NMR spectroscopy, mass spectrometry, and liquid chromatography-mass spectrometry. Details regarding the synthesis and characterizations are included in the supporting information.

CatalyCEST MRI studies in biochemical solution

MRI studies were performed with a Biospec MRI scanner operating at 7 T (300 MHz) magnetic field strength with a 72 mm volume transceiver coil (Bruker Biospin, Inc., Billerica, MA). Images were processed using ParaVision v5.1 software, and CEST MR image analyses were performed with Matlab v8.4 (Mathworks, Natick, MA). For all catalyCEST MRI studies, the temperature of the magnet bore was maintained at 37.0 ± 0.2°C by using an automated temperature feedback system with warmed air (SA Instruments, Inc., Stony Brook, NY).

To perform initial CEST MRI studies, GR-4Am-SA was prepared at 25 mM concentration in phosphate buffered saline (PBS), 3X buffer (pH 7.3). A set of initial images were acquired using a multislice spin echo MRI protocol with the following parameters: TR: 500 ms; TE: 10.0 ms; excitation flip angle: 90°; matrix: 128×128; field of view: 8×8 cm; in-plane spatial resolution: 625×625 μm; slice thickness: 1 mm; number of slices: 30; number of averages: 1; total scan time: 1:04 min. We performed CEST with a Fast Imaging with Steady state Precession (FISP) MRI acquisition protocol with the following parameters: TR: 3.196 ms; TE: 1.598 ms; excitation flip angle: 30°; matrix: 128×128; field of view: 8×8 cm; in-plane spatial resolution: 625×625 μm; slice thickness: 1 mm; number of slices: 1; number of averages: 1 (10). We acquired a series of 85 images with selective saturation from −15 ppm to 15 ppm, in 0.25 ppm increments from 15 ppm to −3 ppm, and 1 ppm increments from −4 ppm to −15 ppm, for a total scan time of 9:07 min. Ten 600 ms square shaped saturation pulses at a saturation power of 4 μT were used at each saturation frequency. Then 50 units of uPA enzyme and dithiothreitol (DTT; 1.5 mg, 9.7 pmol) were added to this solution to provide a reducing environment for enzyme catalysis. The solution was incubated for 12 h at

37°C and catalyCEST MRI studies were performed using the same CEST-FISP MRI protocol. The role of the DTT reducing agent during enzyme catalysis was also evaluated by performing catalyCEST MRI studies on a 25 mM substrate sample solution with only DTT and a similar study with only addition of uPA without DTT.

Other conditions that affect CEST signals were also evaluated. To perform these studies, a 25 mM sample of GR-4Am-SA was used in PBS, 3X buffer, pH 7.3. To optimize saturation power, CEST MRI results were obtained with a saturation time of 6 s and a saturation power ranging from 1 μT to 7 μT. A similar optimization study was performed for saturation time, in which the same sample was used to collect CEST data at 4 μT and saturation times varying from 0.2 s to 7 s. The effect of pH on both the amide and salicylic acid CEST signals of GR-4Am-SA were also studied with 25 mM substrate solutions that had a pH ranging from 6.4 to 7.4. These studies were also performed at 4 μT saturation power and 6 s saturation time.

To analyze each CEST MRI spectrum from a region of interest in an image of GR-4Am-SA, the MR signal at each saturation frequency was normalized to the MR signal with saturation applied at −15 ppm. Then the spectrum was fit to a single function that consisted of a sum of five Lorentzian line shapes to account for four CEST signals at 9.0, 5.0, 3.0 and 1.8 ppm and also to account for the direct saturation of water (8,11). This fitting method was used to obtain the CEST signal amplitudes for each exchangeable proton. The amplitude, width and center of each Lorentzian line were then allowed to change to optimize the fit. This method corrected for potential B_0 inhomogeneities in the CEST MR images, so that additional MRI studies were not needed for measuring B_0 inhomogeneity on a pixelwise basis (12). A correction for possible B_1 inhomogeneity was not performed, because both CEST signals are affected by B_1 inhomogeneity and therefore the ratio of CEST signals is largely unaffected by B_1 inhomogeneity. The reaction coordinates were determined using Eq. [1]. The reaction coordinate is a measure of the progression of the enzyme reaction, where RC = 1 indicates a complete reaction, which provides an estimate of the uPA enzyme activity in the sample (13).

$$\mathrm{RC}=1-\frac{\left[\frac{CEST@5.0\ ppm}{CEST@9.5\ ppm}\right]_{after}}{\left[\frac{CEST@5.0\ ppm}{CEST@9.5\ ppm}\right]_{before}} \quad \text{Eq. [1]}$$

In vivo detection of enzyme activity

All *in vivo* studies were performed with approval from the University of Arizona Institutional Animal Care and Use Committee. To prepare the mouse model of pancreatic cancer, seven female nude mice that were 6 to 8 weeks old were injected with 1×10^6 to 2×10^6 Capan-2 tumor cells suspended in 200 μL to 300 μL of PBS with 50% Matrigel™ (BD Biosciences, Inc.) subcutaneously in the right flank. All imaging studies were performed 35–40 days post injection when the tumor reached approximately 350 mm^3 in diameter.

To perform *in vivo* catalyCEST MRI studies, each mouse was anesthetized with 1.5–2.5% isoflurane delivered in 1 L/min oxygen gas ventilation. The mouse was then secured to a customized MRI–compatible cradle, probes for monitoring rectal temperature and respiration were connected to the mouse, and core body temperature was regulated at 37.0 ± 0.2°C using an air heater (SA instruments, Inc., Stony Brook, NY). An initial set of images were acquired to help locate the tumor, using a multislice spin echo MRI protocol with the following parameters TR: 1200 ms; TE: 21.26 ms; excitation flip angle: 90°; coronal image orientation matrix: 256×128; field of view: 6×4 cm; in-plane spatial resolution: 234×312 μm; slice thickness: 1 mm; number of slices: 17; number of averages: 1; total scan time: 2:33 min. After identifying the tumor location with MRI, the mouse was temporarily removed from the magnet, a solution of 250 mM of GR-4Am-SA in 200 μL of sterile PBS was subcutaneously injected into the mouse within 5 mm of the tumor. After injection of the agent, a 10-minute delay occurred before imaging to allow the agent to be cleaved by enzyme and also for proper equilibration of temperature to 37.0 ± 0.2 °C. The *in vivo* CEST-FISP MRI studies used the following parameters of TR: 3.698 ms; TE: 1.649 ms; excitation flip angle: 15°; with radiofrequency spoiling; centric encoding during acquisition; matrix: 128 ×128; field of view: 6×4 cm; in-plane spatial resolution: 469×312 μm; slice thickness: 2 mm; number of slices: 1; number of averages: 1. Ten 600 ms square shaped saturation pulses at a saturation power of 4 μT were used at each saturation frequency. A series of ten catalyCEST MRI scans were acquired with a series of 47 saturation frequencies at ppm values of +14, +13, +12.6 to 3 (with 0.4 ppm increments), +2.5 to −2.0 (with 0.5 ppm increments), and −3 to −12 (with 3 ppm increments). Ten consecutive CEST spectra were acquired. At the conclusion of the MR scan, the mouse was allowed to recover after being removed from the magnet and cradle.

We then obtained parametric maps of the CEST signal amplitudes during *in vivo* catalyCEST MRI studies. We averaged images from the ten CEST spectra, and applied a Gaussian spatial filter to the average image with a 3×3 pixel matrix and a σ value of one pixel (12). The ROI for the tumor was determined from the anatomical MR images, and the CEST spectra for each pixel in the ROI were obtained from the CEST MR images. Also, linear baseline correction was applied to compensate for power drift of the gradient amplifier, and possible heating of the static shim coils. To analyze the *in vivo* CEST spectra, a function of 7 Lorentzian line shapes was fit to each CEST spectrum to measure the signal amplitudes of the CEST effects at 9.5, 5.0, 3.0 and 1.8 ppm and also to account for direct saturation of water and the endogenous effects of amide proton transfer and magnetization transfer. The center frequency, width and amplitude of all Lorentzian line shapes were allowed to change. The parametric maps of the reaction coordinates were determined using Eq. [2] to provide estimates of the uPA enzyme activity (14).

$$\mathrm{RC}=1-\frac{[CEST@5.0\ ppm]_{after}}{[CEST@9.5\ ppm]_{after}} \quad \text{Eq. [2]}$$

Notably, Eq. [1] and Eq. [2] are the same when $[\text{CEST @ 5.0 ppm}]_{\text{before}} = [\text{CEST @ 9.5 ppm}]_{\text{before}}$. In addition, CEST spectra were obtained for the ROI of each tumor by averaging

the images, applying a Gaussian spatial filter, linear baseline fitting to account for power drift of the gradient amplifier, and averaging the CEST spectra of the pixels in the ROI. The same Lorentzian line shape fitting method was applied to each of these CEST spectra of each ROI.

RESULTS

Synthesis of the CEST agent

The contrast agent, GR-4Am-SA, was synthesized in an overall yield of 23%, following a straightforward synthesis strategy (Fig. S1). After protecting the acid and hydroxyl functional groups of 4-amino salicylic acid, the arginine and glycine amino acids were coupled to the amino group following standard peptide coupling procedures. The agent was deprotected and purified for our catalyCEST MRI studies. The facile 5-step synthesis of GR-4Am-SA improved on our 7-step synthesis of a paramagnetic CEST agent that also detected uPA activity.

Detection of uPA activity in biochemical solution

Initial catalyCEST MRI studies detected four CEST signals from GR-4Am-SA at 9.5, 5.0, 3.2, and 1.8 ppm (relative to the water resonance defined to be 0 ppm for MRI studies; Fig. 3a). These CEST signals were assigned to the salicylic acid proton, the aryl amide proton, the aliphatic amide group, and the guanidinium group, respectively, based on previous reports (8,14–16). Only the CEST signals at 5.0 ppm and 9.5 ppm of GR-4Am-SA were important for our current study, and the other two CEST signals were not analyzed further.

A solution of 25 mM of GR-4Am-SA was incubated with 20 units (384 pmol) of uPA enzyme for 12 hours in the presence of DTT to maintain reducing conditions. After the reaction, the solution was analyzed using CEST MRI (Fig. 3a). The CEST signal amplitude at 9.5 ppm showed relative stability by increasing only 12%, indicating that this CEST signal could serve as a control that is unresponsive to uPA activity (throughout this report, the increase or decrease in CEST signal amplitude is reported as a percentage of the original value, and the increase or decrease is not reported as an absolute % CEST value). The CEST signal amplitude at 5.0 ppm decreased by 69%. These changes in CEST signals resulted in a reaction coordinate of 76.1% using Eq. [1], demonstrating that GR-4Am-SA can detect uPA activity with catalyCEST MRI.

To verify that uPA requires a reducing environment to function, we added 20 units of the enzyme to a 25 mM solution of GR-4Am-SA without DTT, which was incubated overnight and then analyzed with CEST MRI (Fig. 3b). The CEST signals decreased by a relatively minor 16% and 15% at 9.5 and 5.0 ppm, respectively. Moreover, the reaction coordinate was determined to be 3.3%, indicating that the uPA enzyme was largely inactive without DTT. To verify that DTT did not affect GR-4Am-SA, we added DTT to a 25 mM solution of the contrast agent without enzyme, and incubated the solution overnight before performing catalyCEST MRI (Fig. 3c). The CEST signals only decreased by 2% and 15% at 9.5 and 5.0 ppm, respectively, resulting in an effective reaction coordinate of 12.4%, demonstrating that GR-4Am-SA has good stability in reducing conditions.

Evaluation of CEST MRI conditions

We assessed the effects of saturation power and saturation time on CEST signal amplitudes of GR-4Am-SA to optimize the catalyCEST MRI protocol for subsequent *in vivo* CEST MRI studies. The Hanes-Woolf QUantifying Exchange using Saturation Power (HW-QUESP) method was used to determine that a saturation power of 4 μT generated a strong 4.75% CEST signal from the salicylic acid proton, and 8.6% CEST signal from the aryl amide proton (Fig. 4a,b) (17). A saturation power of 4 μT is a safe power level for *in vivo* imaging, so that this power was used for subsequent *in vivo* studies (18). The Reverse Linear Quantifying Exchange using Saturation Time (RL-QUEST) method was used to assess the effect of saturation time, which showed that a saturation time of 3 s generated a maximum CEST signal from both protons (Fig. 4c,d) (19). To ensure steady state saturation during our subsequent *in vivo* studies, we set the saturation time to 6 s for our subsequent *in vivo* studies.

The HW-QUESP linear analysis method was then used to calculate the chemical exchange rates for the amide proton at 5 ppm and the salicylic acid proton at 9.5 ppm of GR-4Am-SA (17). This analysis method compensates for inaccurate saturation power caused by B_1 inhomogeneities. The exchange rates of 345 Hz for the amide proton and 835 Hz for salicylic acid were found to be comparable to that for similar compounds (14–16). We did not use the RL-QUEST method to generate chemical exchange rates because this analysis method requires high concentrations of the agent for accurate estimates (19).

We also evaluated the effect of pH on CEST signal amplitudes of GR-4Am-SA. The CEST signal for the amide proton increased with increasing pH which was expected because the chemical exchange of an amide proton is base catalyzed (20). The CEST signal for the salicylic acid proton increased with increasing pH until 7.0 after which we observed a decrease in the CEST signal amplitude with higher pH. This result was also expected because the chemical exchange rate of salicylic acid becomes rapid at higher pH, which causes MR coalescence of the resonances of salicylic acid and water, which reduces the resonance at 9.5 ppm that can be saturated (21). Overall, these results showed that stronger CEST signals can be detected under mildly acidic or neutral physiological conditions, relative to strongly acidic physiological conditions. Solid tumors are often mildly acidic, because tumor cells often have enhanced aerobic glycolysis that produces excess lactic acid, known as the Warburg effect (22). Therefore, the CEST effect of GR-4Am-SA has a dependence on pH that is well suited for the study of solid tumors.

In vivo catalyCEST MRI studies

Our initial *in vivo* catalyCEST MRI studies used a xenograft flank model of a Capan-2 pancreatic tumor that had been previously shown to have high uPA activity (Fig. 5) (9). These studies demonstrated an average of 10.6% CEST signal at 9.5 ppm from GR-4Am-SA within the tumor region of seven mice, which indicated good uptake of the agent into the tumor. The standard deviation of the CEST signal at 9.5 ppm was 2.8% with a range of 6.0% to 13.3%. The CEST signal from GR-4Am-SA in tissues around the tumor was negligible, which indicated that the agent was not retained in these tissues during the time course of our MRI studies. The average CEST signal at 5.0 ppm from GR-4Am-SA for all mice was 2.2%,

indicating that much of the aryl amide had been converted to an amine *in vivo*. The standard deviation of this CEST signal was 1.0% with a range of 0.8% to 3.3%. A paired Student's t-test showed that the CEST signals at 9.5 ppm and 5.0 ppm were statistically different (P = 0.00006).

The reaction coordinate was determined from the ratio of CEST signals at 5.0 ppm relative to 9.5 ppm using Eq. [2]. The average reaction coordinate was 79.7%, with a standard deviation of 7.5% and a range of 70.4% to 89.6%. Again, these results showed that all tumors had consistently high enzyme activity, although with a moderate range of high activities. Importantly, the reaction coordinate was more dependent on the enzyme-responsive CEST signal at 5.0 ppm, as shown by a R correlation coefficient of 0.91 (Fig. 6a). The reaction coordinate is a dependent variable that depends on the two CEST signals (which are independent variables), which justifies the use of a "R" correlation coefficient to assess dependency of one variable on another variable, relative to the commonly used R^2 correlation coefficient for comparing two independent variables (23). For comparison, the reaction coordinate had a relatively weak dependence on the enzyme-unresponsive CEST signal at 9.5 ppm (R = 0.32; Fig. 6b). This result shows that the reaction coordinate is largely independent of the concentration of GR-4Am-SA that is tracked by the CEST signal amplitude at 9.5 ppm.

DISCUSSION

In this study, we have shown that catalyCEST MRI can use GR-4Am-SA to detect uPA activity in biochemical solution. This approach with a single diamagnetic CEST agent improves on our previous studies of two paramagnetic CEST agents. The ratio of CEST signals on the single GR-4AM-SA agent can assess enzyme activity in a concentration-independent manner in biochemical solution and *in vivo*. For comparison, the two paramagnetic agents used in our previous study may have different pharmacokinetic delivery to tumor tissues, compromising a concentration-independent measurement of enzyme activity. Furthermore, our diamagnetic CEST agent could be administered *in vivo* at a higher concentration than paramagnetic CEST agents, which improved detection sensitivity. A clinically-acceptable saturation power of 4 μT was used with our diamagnetic CEST agent; a higher 10 μT saturation power was required to detect our paramagnetic CEST agent, which is likely too powerful for eventual clinical studies (9,18). For these reasons, GR-4Am-SA has better potential for clinical translation to monitor uPA activity levels within patients who have solid tumors.

Enzymes are notoriously promiscuous and cleave multiple substrates, which can compromise the specificity for detecting the activity of an intended enzyme (24). In our study, proteases other than uPA may have cleaved the peptidyl ligand of GR-4Am-SA during *in vivo* studies of the Capan-2 tumor model. Furthermore, our biochemical studies indicated that uPA only actively catalyzed cleavage of GR-4Am-SA under reducing conditions. An *in vivo* tumor microenvironment that is oxidative or redox-neutral may have reduced uPA activity for GR-4Am-SA, while uPA activity may still be high for catalyzing the cleavage of other proteins in the same microenvironment. Similarly, our biochemical studies showed that the CEST signals of GR-4Am-SA are strongest at mildly acidic or neutral pH. A highly

acidic *in vivo* tumor microenvironment may have weaker CEST signals that could compromise the detection of high uPA activity. Finally, CEST signal amplitudes for our type of diamagnetic CEST agent are approximately linear with agent concentration only for CEST signals that are 10% or lower (8,13). Future studies should evaluate the CEST signal-concentration calibration to more accurately estimate the reaction coordinate. Therefore, further studies are warranted that detect other enzyme activities, assess the redox state, and measure the acidity within tumor models (25, 26). Yet our demonstration of the *in vivo* uPA activity in the Capan-2 tumor model with GR-4Am-SA and catalyCEST MRI contributes to the armamentarium of cancer imaging techniques that can interrogate the tumor microenvironment.

Supplementary Material

Refer to Web version on PubMed Central for supplementary material.

Acknowledgments

Sponsors: The research was supported by through the NIH through grants R01CA169774 and P30CA023074.

The authors would like to thank the Experimental Mouse Shared Resource of the University of Arizona Cancer Center for preparing the mouse model. The research was supported by through the NIH through grants R01CA169774 and P30CA023074.

Abbreviations

CEST	Chemical Exchange Saturation Transfer
DTT	dithiothreitol
FISP	Fast Imaging with Steady state Precession
HW-QUESP	Hanes-Woolf QUantifying Exchange using Saturation Power
PBS	phosphate buffered saline
RL-QUEST	Reverse Linear Quantifying Exchange using Saturation Time
ROI	region of interest
uPA	urokinase Plasminogen Activator

References

1. Andreasen PA, Kjoller L, Christensen L, Duffy MJ. The urokinase-type plasminogen activator system in cancer metastasis: a review. Int J Cancer. 1997; 72:1–22. [PubMed: 9212216]
2. Zou Z, Zeng F, Xu W, Wang C, Ke Z, Wang QJ, Deng F. PKD2 and PKD3 promote prostate cancer cell invasion by modulating NF-κB-and HDAC1-mediated expression and activation of uPA. J Cell Sci. 2012; 125:4800–4811. [PubMed: 22797919]
3. Duffy MJ. The role of proteolytic enzymes in cancer invasion and metastasis. Clin Exp Metastas. 1992; 10:145–155.
4. Benraad TH, Geurts-Moespot J, Grondahl-Hansen J, Schmitt M, Heuvel J, De Witte JH, Foekens JA, Leake RE, Brünner N, Sweep CGJ. Immunoassays (ELISA) of urokinase-type plasminogen activator (uPA): report of an EORTC/BIOMED-1 Workshop. Eur J Cancer. 1996; 32:1371–1381.

5. Josan JS, De Silva CR, Yoo B, Lynch RM, Pagel MD, Vagner J, Hruby VJ. Fluorescent and lanthanide labeling for ligand screens, assays, and imaging. Methods Molec Biol. 2011; 716:89–126. [PubMed: 21318902]
6. Daryaei I, Pagel MD. Double agents and secret agents: the emerging fields of exogenous chemical exchange saturation transfer and T2-exchange magnetic resonance imaging contrast agents for molecular imaging. Res Rep Nuc Med. 2015; 15:19–32.
7. Yoo B, Pagel MD. A PARACEST MRI contrast agent to detect enzyme activity. J Am Chem Soc. 2006; 128:14032–14033. [PubMed: 17061878]
8. Hingorani DV, Randtke EA, Pagel MD. A catalyCEST MRI contrast agent that detects the enzyme-catalyzed creation of a covalent bond. J Am Chem Soc. 2013; 135:396–6398.
9. Yoo B, Sheth VR, Howison CM, Douglas MJ, Pineda CT, Maine EA, Baker AF, Pagel MD. Detection of in vivo enzyme activity with catalyCEST MRI. Magn Reson Med. 2014; 71:1221–1230. [PubMed: 23640714]
10. Shah T, Lu L, Dell K, Pagel MD, Griswold M, Flask CA. CEST-FISP: A novel technique for rapid chemical exchange saturation transfer (CEST) MRI at 7T. Magn Reson Med. 2011; 65:432–437. [PubMed: 20939092]
11. Sheth VR, Liu G, Li Y, Pagel MD. Improved pH measurements with a single PARACEST MRI contrast agent. Contrast Media Molec I. 2012; 7:26–34.
12. Chen LQ, Randtke EA, Jones KM, Moon BF, Howison CM, Pagel MD. Evaluations of tumor acidosis within in vivo tumor models using parametric maps generated with acidoCEST MRI. Mol Imaging Biol. 2015; 17:488–496. [PubMed: 25622809]
13. Sinharay S, Randtke EA, Jones KM, Howison CM, Chambers SK, Kobayashi H, Pagel MD. Noninvasive detection of enzyme activity in tumor models of human ovarian cancer using catalyCEST MRI. Magn Reson Med. 2016; doi: 10.1002/mrm.26278
14. Hingorani DV, Montano LA, Randtke EA, Lee YS, Cárdenas-Rodríguez J, Pagel MD. A single diamagnetic catalyCEST MRI contrast agent that detects cathepsin B enzyme activity by using a ratio of two CEST signals. Contrast Media Molec I. 2016; 11:130–138.
15. Yang X, Song X, Li Y, Liu G, Ray Banerjee S, Pomper MG, McMahon MT. Salicylic acid and analogues as diaCEST MRI contrast agents with highly shifted exchangeable proton frequencies. Angew Chem Int Ed. 2013; 52:8116–8119.
16. Yang X, Yang X, Yadav NN, Song X, Ray Banerjee S, Edelman H, Minn I, van Zijl PCM, Pomper MG, McMahon MT. Tuning phenols with Intra-Molecular bond Shifted HYdrogens (IM-SHY) as diaCEST MRI contrast agents. Chem Eur J. 2014; 20:15824–15832. [PubMed: 25302635]
17. Randtke EA, Chen LQ, Corrales LR, Pagel MD. The Hanes-Woolf Linear QUESP method improves the measurements of fast chemical exchange rates with CEST MRI. Magn Reson Med. 2014; 71:1603–1612. [PubMed: 23780911]
18. Liu G, Song X, Chan KWY, McMahon MT. Nuts and Bolts of CEST MR imaging. NMR Biomed. 2013; 26(7):810–828. [PubMed: 23303716]
19. Randtke EA, Chen LQ, Pagel MD. The reciprocal linear QUEST analysis method facilitates the measurements of chemical exchange rates with CEST MRI. Contrast Media Molec I. 2014; 9:252–258.
20. Liepinsh E, Otting G. Proton exchange rates from amino acid side chains—implications for image contrast. Magn Reson Med. 1996; 35:30–42. [PubMed: 8771020]
21. Liu G, Li Y, Sheth VR, Pagel MD. Imaging in vivo extracellular pH with a single PARACEST MRI contrast agent. Molec Imaging. 2012; 11(1):47–57. [PubMed: 22418027]
22. Chen LQ, Pagel MD. Evaluating pH in the extracellular tumor microenvironment using CEST MRI and other imaging methods. Adv Radiol. 2015:206405. [PubMed: 27761517]
23. Everitt, BS. Cambridge Dictionary of Statistics. 4. New York: Cambridge University Press; 2002.
24. Khersonsky O, Tawfik DS. Enzyme promiscuity: a mechanistic and evolutionary perspective. Annu Rev Biochem. 2010; 79:471–505. [PubMed: 20235827]
25. Yoo B, Pagel MD. An overview of responsive MRI contrast agents for molecular imaging. Front Biosci. 2008; 13:1733–1752. [PubMed: 17981664]
26. Hingorani DV, Bernstein AS, Pagel MD. A review of responsive MRI contrast agents: 2005–2014. Contrast Media Molec I. 2015; 10(4):245–265.

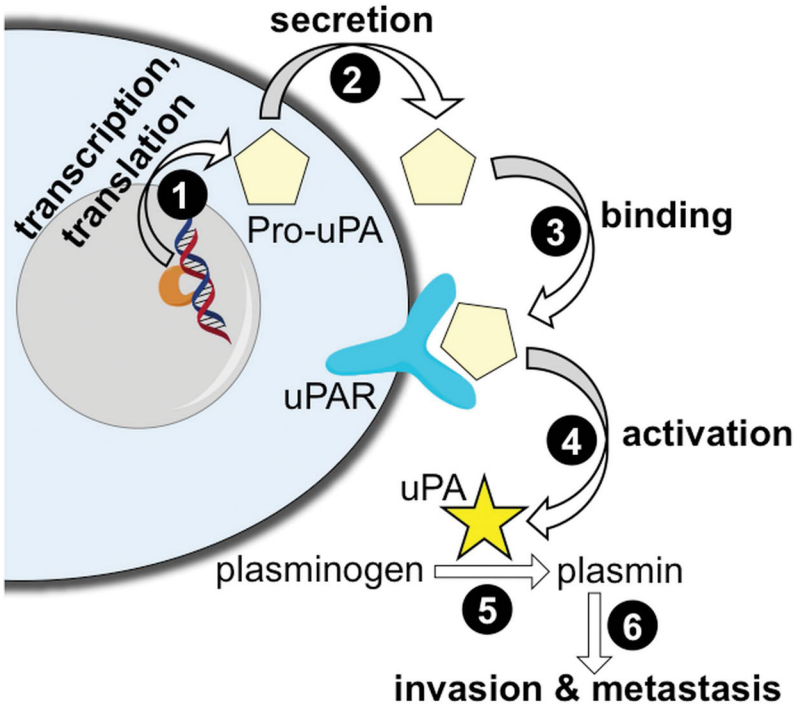

Figure 1.

A schematic of the expression, activation, and function of urokinase Plasminogen Activator (uPA). The inactive pro-uPA zymogen is transcribed and translated (step 1), and eventually secreted from the cell (step 2). After binding to the uPAR receptor (step 3), the pro-uPA is cleaved to become an active uPA enzyme (step 4). uPA can catalyze the conversion of plasminogen to plasmin (step 5), and plasmin then participates in processes that promote tumor invasion and metastases (step 6).

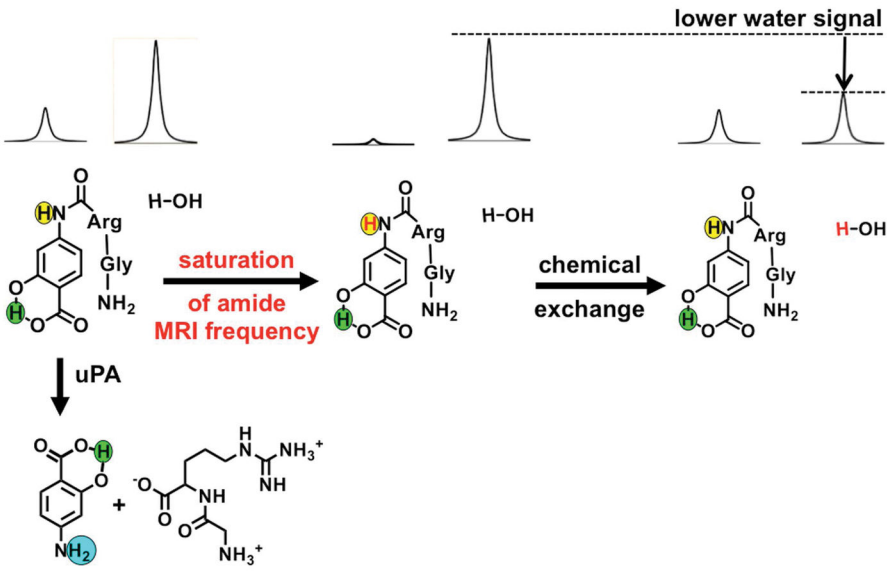

Figure 2.

The catalyCEST MRI mechanism. Top left: The aryl amide (highlighted in yellow) and the water proton have MR signals at distinct frequencies. Center: Selective saturation of the MR frequency of the amide proton causes a loss of the proton's MR signal. Right: Chemical exchange of the amide and water protons transfers the saturation to water, leading to loss of the MR water signal. Bottom left: The CEST effect of the aryl amide proton is lost when uPA cleaves the peptidyl ligand to create an aryl amine (highlighted in cyan). The salicylic acid proton (highlighted in green) can generate a CEST effect, and is unresponsive to enzyme activity.

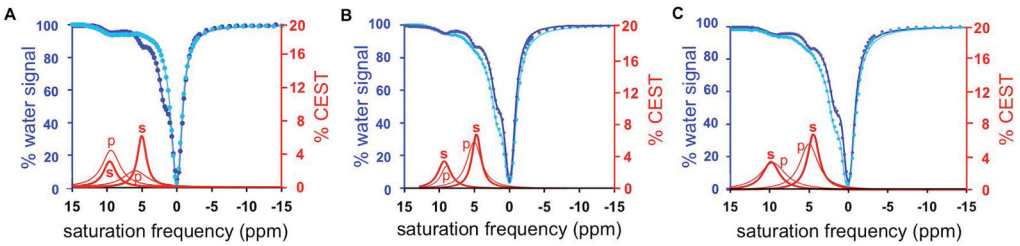

Figure 3.

CatalyCEST MRI of uPA activity. (A) 25 mM of the agent was incubated with 50 units of urokinase Plasminogen activator (uPA) enzyme and 9.7 pmol DTT for 12 hours at 37°C, resulting in a 3.7-fold decrease in the CEST signal amplitude at 5.0 ppm relative to 9.5 ppm. (B) The same experiment without DTT showed almost no change in CEST signals, indicating that DTT was necessary for uPA activity. (C) The same experiment without enzyme showed almost no change in CEST signals, indicating that the agent was stable in a reducing environment with DTT. CEST spectra were acquired by applying selective saturation at 4 μT for 6 s before acquiring a FISP MR image, at 85 selective frequencies spanning 15 to −15 ppm. Experimental CEST spectra are shown as blue circles, the fitting of the experimental spectra are shown as blue lines, and the CEST lineshape spectra from these fittings are shown as red lines. Results for the substrate before adding enzyme are shown as dark lines and labeled with a “s”, while results for the product after adding enzyme are shown as light lines and labeled with a “p”, respectively.

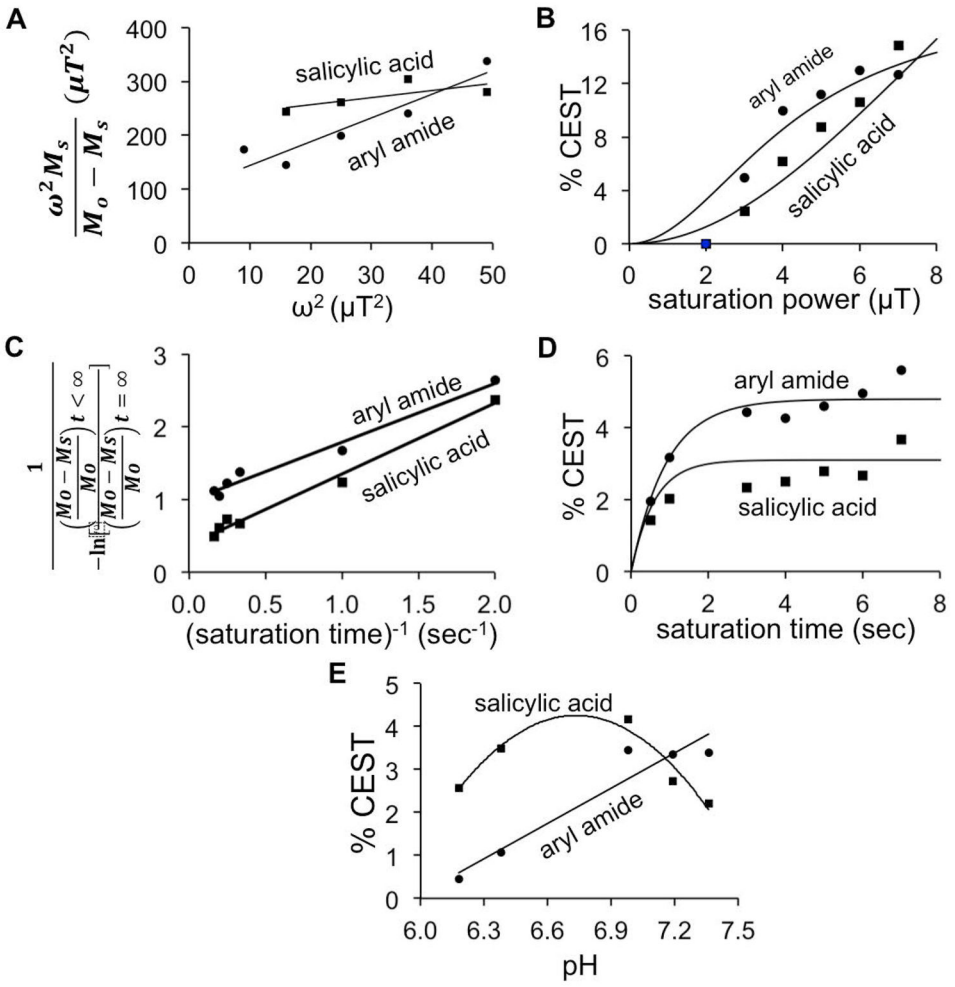

Figure 4.

The effect of saturation power, time, and pH on CEST. (A) A linear HW-QUESP plot was used to analyze the relationship between saturation power and CEST signal amplitude for the aryl amide and salicylic acid protons, using a saturation time of 6 s. (B) This analysis was used to plot the non-linear relationship between saturation power and CEST signal. (C) A linear RL-QUEST plot was used to analyze the relationship between saturation time and CEST signal amplitude for the aryl amide and salicylic acid protons, using a saturation power of 4 μT. (D) This analysis was used to plot the non-linear relationship between saturation time and CEST signal. (E) The CEST signal amplitudes of the two exchangeable protons were dependent on pH. For these results with pH, lines are only included to aid the visualization of the experimental data, and these lines do not fit an experimental model. CEST spectra were acquired by applying selective saturation 85 selective frequencies spanning 15 to −15 ppm.

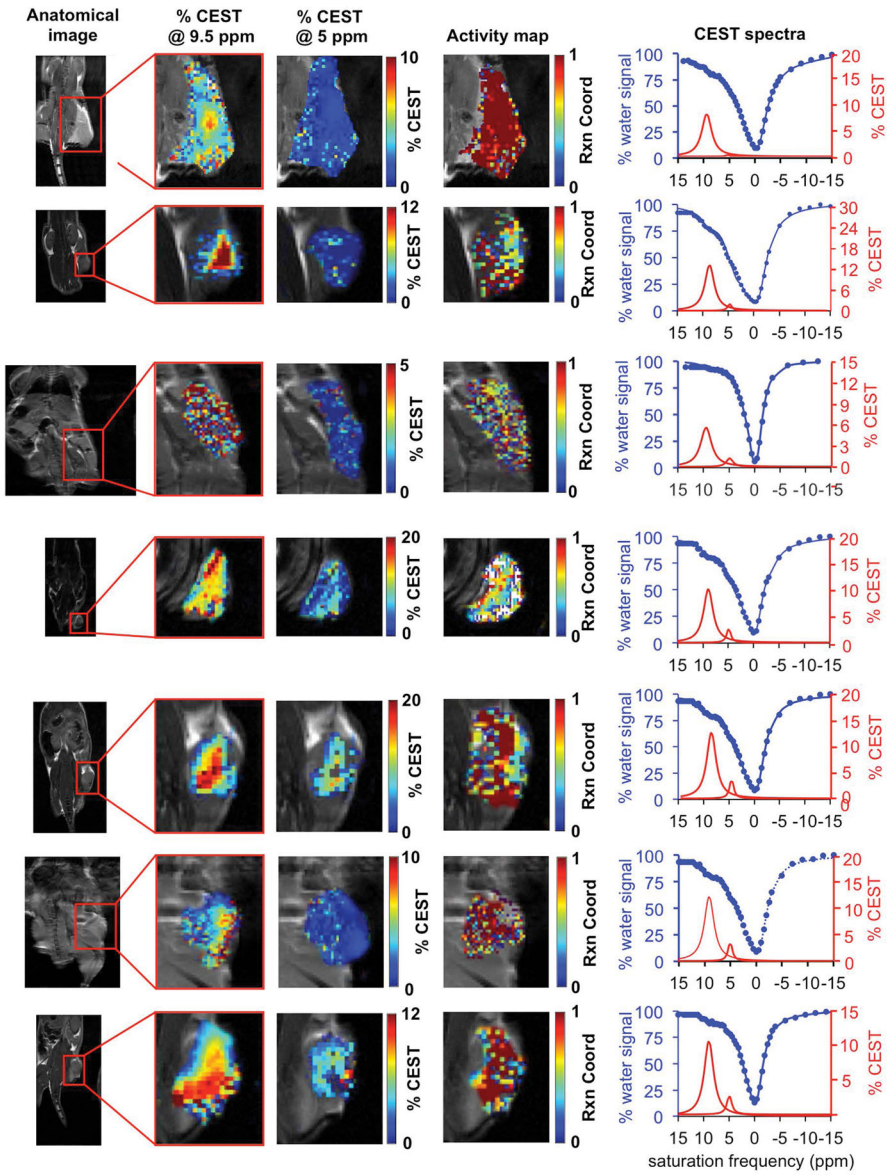

Figure 5.

In vivo catalyCEST MRI of uPA activity. A tumor model of Capan-2 pancreatic cancer showed high activity of urokinase Plasminogen activator (uPA). For each study, the xenograft flank tumor was identified with anatomical MRI, % CEST signal amplitudes at 9.5 ppm and 5 ppm were measured on a pixelwise basis, and an activity map of the uPA reaction coordinate were constructed using Eq. [2]. The CEST spectra of the tumor regions are also shown. CEST spectra were acquired by applying selective saturation at 4 μT for 6 s before acquiring a FISP MR image, at 85 selective frequencies spanning 15 to −15 ppm. Experimental CEST spectra are shown as blue circles, the fitting of the experimental spectra are shown as blue lines, and the CEST line shape spectra from these fittings are shown as red lines.

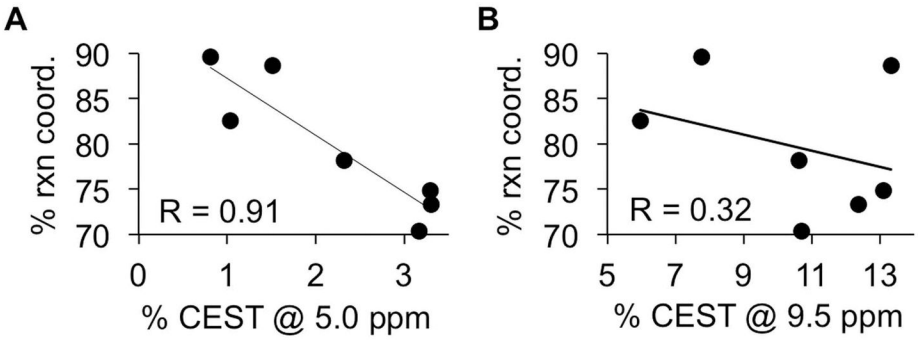

Figure 6.

The dependence of the reaction coordinate on CEST signal amplitudes. (A) The reaction coordinate showed a linear dependence on the CEST signal at 5.0 ppm, with an R correlation coefficient of 0.91. (B) The reaction coordinate was largely independent of the CEST signal at 9.5 ppm, with an R correlation coefficient of 0.32.